Optimisation of Auxiliary Transmitter Placement in a Dual-Mode X-Band FMCW Harmonic Radar

Alfonso Capitano - S2324849 - University of Twente - EEMCS Faculty - Radio Systems

***Abstract*—In modern radar applications utilising multiple independent transmitters, optimisation challenges arise due to various complex signal interactions. This is especially so in non-linear radar systems that rely on non-linear properties of the target to produce a return signal at a frequency different from that of the illuminating signals. The aim of this thesis is to improve the coverage area of an existing non-linear harmonic radar setup through the utilisation of multiple auxiliary transmitters (helpers) and the optimisation of their placement. Using the same power budget and equal transmit power distribution, the results presented in this work indicate that adding one helper transmitter increases coverage area by roughly 35.8% in comparison to the stand-alone conventional harmonic radar system. Coverage area can increase with 37.0%, 44.4%, 54.3% and 59.3%, by utilising 2, 3, 4 and 5 helper nodes, respectively. Using multiple low-power transmitters is less costly than a single high-power transmitter, making the use of auxiliary transmitters a more cost-effective solution to increase coverage area.**

I INTRODUCTION

Radio detection and ranging (radar) systems emit electromagnetic (EM) waves, and receive reflections from objects in their field of view. This is mainly applied to determine the location, motion or speed of an object [1]. In some applications, conventional radar suffers from clutter. Clutter makes it difficult to isolate the target signal of interest due to unwanted reflections from other objects. What constitutes clutter is largely dependent on the application of the radar, e.g. movement by sea waves create clutter for marine radar [2].

To mitigate clutter, the transmit and receive frequency bands are separated using non-linear radar, such as harmonic radar. In harmonic radar, the return signal is a harmonic of the frequency used to transmit. However, such a system requires a non-linear target capable of generating these harmonics, e.g. oxidated pieces of metal or semiconductors such as diodes. This target reflects harmonics of incident signals, enabling suppression of clutter as it remains at the transmit frequency [3].

When there are several signal sources operating at different frequencies, non-linear targets generate both harmonic return and intermodulation reflected signals. A dual-mode system can utilise both [4]. This is done using auxiliary transmitters with frequencies slightly offset from the main radar, but within the same band.

This work is about optimising the coverage area of a dual-mode X-band frequency modulated continuous wave (FMCW) harmonic radar using auxiliary transmitters, where X-band is the operation range from 8 to 12 GHz [5]. Using both harmonic and intermodulation signals, the radar can achieve a higher maximum detection range while using cheap and simple single carrier transmitters [6].

When multiple independent transmitters are used, the resulting signals affect each other, e.g. in terms of phase and amplitude interference. Optimal placement of these transmitters thus becomes a combinatorial problem that grows with the number of transmitters used and the area under investigation. The objective of this work is to maximise coverage area when considering both the harmonic and intermodulating signal returns. Since the intermodulation signal is the result of mixing two signals from the main radar and the auxiliary transmitters, all placement combinations need to be considered for a comprehensive result in optimisation.

To reach the objective, a software optimiser is designed and used. This optimiser is able to use multiple input parameters, such as the transmitter position and antenna orientation, for a varying number of helper nodes. It is realised through use of a MATLAB simulation model which is verified through experimental data for one helper. The results of the optimiser are expressed in area coverage and its increase. All evaluations are done using equal total power budgets to make the comparison easier and more fair.

Necessary background information on non-linear radar, specifically harmonic radar (HR) and intermodulation radar (IR), is provided in Section II. Section III introduces the provided initial simulation model, detailing single helper and multiple helper set-up configurations and calculations. In Section IV, the improvements made to the initial simulation model are discussed, starting with a single helper before moving to a multiple helper configuration. Section V discusses helper placement optimisation. A problem statement is given before presenting an optimisation approach using simulated annealing. Section VI presents the results of the designed optimiser, followed by a discussion on the findings and possible improvements in Section VII. Lastly, Section VIII concludes the report with a summary on key findings. Additional materials are included in the appendices, such as the glossary in Appendix A which is provided for convenience.

II BACKGROUND

II-A *Harmonic Radar*

Harmonic radars work on the principle that the target exhibits non-linear properties when they are illuminated with a radar signal, e.g. intermodulation effects and a non-linear output response. One such target is called a tag. It contains an antenna and a non-linear device, such as a Schottky diode. It uses a transmitted signal illuminating its antenna as an energy source and re-emits harmonics of the transmitted frequency [7]. The power level of the non-linear response is thus dependent on the conversion loss provided by the tag.

This thesis is built on the set-up proposed in [4] and [6], namely a dual-mode FMCW harmonic radar that is capable of receiving both harmonic and intermodulation terms simultaneously. The set-up uses a tag consisting of a half-wavelength planar dipole antenna, a low barrier Schottky diode (SMS7621) and a small inductive loop [6].

Modelling the response of a generic non-linear target as a power series yields [4]:

$$E_{\text{out}}(t) = \sum_{n=1}^{\infty} k_n E_{\text{in}}^n(t) = \sum_{n=1}^{\infty} E_n(t), \tag{1}$$

where $E_{\text{in}}(t)$ is the incident electric field, $E_{\text{out}}(t)$ is the reflected electric field, k_n is the power-series coefficients that depend on the target and $E_n(t) = k_n\, E^n_{\text{in}}(t)$. Using a passband input in the form of $E_{\text{in}}(t) = A\,\text{Re}\{\, s(t)\, e^{j2\pi f_c t}\}$, where $s(t)$ is a baseband complex envelope signal and A is the signal amplitude. Then the nth power term in (1) is written as:

$$E_n(t) = k_n \sum_m h_{m,n} A^n \text{Re}\Big\{ s^m(t)|s(t)|^{n-m}\, e^{j2\pi\, m\, f_c\, t}\Big\}, \quad (2)$$

where $h_{m,n}$ is a combinatorial coefficient whose value can be found in [4]. Assuming for simplicity that $s(t)$ has unit magnitude (e.g., a constant amplitude for nth power term or suitably normalized waveform), equation (2) is further simplified to

$$E_n(t) \;=\; k_n \sum_m h_{m,n}\, A^n\, \text{Re}\Big\{ s^m(t)\, e^{j2\pi\, m\, f_c\, t}\Big\}. \quad (3)$$

The radar transmitter emits a radio frequency (RF) compressed high-intensity radiated pulse (chirp) signal at some fundamental frequency f_1, and the receiver detects returns at the harmonic frequencies mf_1. As the amplitude of the harmonics decreases with m, the strongest harmonic, which is the second-harmonic, is commonly chosen for system design. At low incident power, the target response is dominated by the $n = m$ term. This simplifies the second-harmonic response to:

$$E_{\text{ref}}(t) \;=\; 0.5\, k_2\, A^2\, \text{Re}\{\, s^2(t)\, e^{j2\pi\,(2f_1)\,t}\}, \quad (4)$$

where k_2 is dependent on the target properties.

II-B Intermodulation Radar

With IR the target is illuminated by multiple RF signals. The first signal is the main radar's chirp signal at carrier f_1, the second signal is an auxiliary single-tone carrier at f_2. A baseband complex envelope signal with carrier frequency f_1 and a single tone transmitter with carrier frequency f_2 are used to describe these incident electric field, respectively:

$$\begin{aligned} E_{\text{in}1}(t) \;&=\; A_1\, \text{Re}\{\, s_1(t)\, e^{j2\pi f_1\, t}\}, \\ E_{\text{in}2}(t) \;&=\; A_2\, \text{Re}\{1(t) e^{j2\pi f_2\, t}\}. \end{aligned} \quad (5)$$

To ensure that the components for IR and HR do not overlap, it is required that $f_2 > f_1 + \Delta f$, where $\Delta f = 3B/2$ and B is the bandwidth of $s_1(t)$. The electric field going into the tag is described as:

$$E_{\text{in}}(t) \;=\; E_{\text{in}1}(t) \;+\; E_{\text{in}2}(t). \quad (6)$$

Using the same approach as in (3), the return signal will contain four second order mixing products:

- a harmonic chirp signal with bandwidth $2B$ centred around $2f_1$;
- a harmonic of the single-tone signal with bandwidth $2B$ centred around $2f_2$;
- two intermodulation product chirp signals of bandwidth B, centred around $f_1 + f_2$ and $f_2 - f_1$.

The resulting reflected field is described by:

$$\begin{aligned} E_{\text{ref}}(t) = \frac{k_2}{2} \Big[& A_1^2\, \text{Re}\{s_1^2(t) e^{j4\pi f_1 t}\} \\ & + A_2^2\, \text{Re}\{1(t) e^{j4\pi f_2 t}\} \\ & + 2\, A_1 A_2\, \text{Re}\{s_1(t)\, e^{j2\pi (f_1+f_2)t}\} \\ & + 2\, A_1 A_2\, \text{Rr}\{s_1(t)\, e^{j2\pi (f_2-f_1)t}\}\Big]. \end{aligned} \quad (7)$$

When the amplitudes of the incident signals in (7) are equal, the second order intermodulation products yield 6 dB higher reflected power than just the harmonic reflections.

Figure 1 describes the power ratio of the reflected intermodulating power over the harmonic power using (7). At lower incident

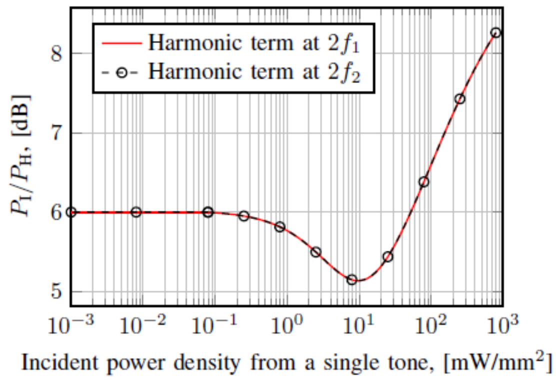

Fig. 1: Received power of the intermodulation term F_I relative to the received power of the harmonic terms F_H as a function of the incident power density on the non-linear target [4].

power, the received power of the intermodulation products are measured to be 6 dB larger than the harmonic products. Low power application is considered, therefore higher power incident density from the auxiliary transmitters is beyond the scope of this work.

III Initial Simulation Model

III-A Single helper set-up

A simulation model using an integrated graphical user interface (GUI) was provided at the start of the thesis. The GUI is a MATLAB application that calculates the return signals from a harmonic tag in response to two independent input signals, which are the main radar signal and the auxiliary helper signal. The two input signals each get assigned parameters, (e.g. centre frequency, transmission power, position, antenna gain and antenna orientation). After this, the tag position is iterated in steps over a grid to calculate the power of the signal return products at distances d_1 and d_2 from the first and second transmission antenna positions, respectively. Using the transmission signals as its input, the calculated signals are the main radar harmonic return when no auxiliary transmitters are present, the main radar harmonic return with added helper nodes and the intermodulation signal. The power of the return signals is calculated and the three outputs are presented in the form of a heat map. The total power used in the system from [6] is a distributed 100 Watt for the main radar and 100 Watt for the helpers. All parameters that can be set and the input parameters used as a verification metric are recorded in Table I. A screenshot of the GUI can be seen in Appendix B, Figure B.1.

TABLE I: Table containing all input parameters and options contained in the GUI for reference

Symbol	Description	Value	Unit
X	Range of the grid	120	m
dX	Calculation resolution	5	m
$P_{\text{Rx,min}}$	Minimal power threshold value (optional)	(-70)	dBm
f_1	Centre carrier frequency of main radar	9.34	GHz
$P_{\text{Tx,main}}$	Transmission power of main radar	50	dBm
$G_{\text{Tx,main}}$	Transmission gain of main radar	15	dBi
$G_{\text{Rx,main}}$	Return signal gain of main radar	15	dBi
$X_{\text{main}}, Y_{\text{main}}$	Position of main radar	0,60	m
θ	Orientation of main radar	0	°
f_2	Carrier frequency of helper nodes	9.5	GHz
$P_{\text{Tx,helper}}$	Transmission power of helper nodes	50	dBm
$G_{\text{Tx,helper}}$	Transmission gain of helper nodes	15	dBi
X_h, Y_h	Position of helper nodes	120,60	m
θ_h	Orientation of helper nodes	180	°
N.A.	Gain patterns for main radar and helper-transmission and return signals (optional)	(Horn)	dBi

The GUI is built on the experimental results obtained from [6]. The signal power going into the tag from the radar at a given point in space a distance d away can be calculated using:

$$P_{\text{in}} = P_{\text{tx}} + G_{\text{tx}} - \text{FSPL}(d, f) + G_{\text{in,D}}, \tag{8}$$

where P_{tx} is the transmit power of the radar transmitter, G_{tx} is the transmit gain of the radar transmitter, FSPL is the free space path loss and $G_{in,D}$ is the tag input antenna gain. The amplitudes of the incoming signals are obtained from the power going into the tag at a given point in space after accounting for the FSPL:

$$\text{FSPL}(d, f) = \left(\frac{c}{4\pi f d}\right)^2 = \left(\frac{\lambda}{4\pi d}\right)^2, \tag{9}$$

where d is the distance from the transmitting antenna to the tag and $\lambda = c/f$ is the wavelength. Converting P_{in} to linear power, allows a single electric field input amplitude to be obtained using the impedance of the tag Z_{f_1} at fundamental frequency f_1:

$$V_{in}(t) = \sqrt{P_{\text{in}} \cdot \text{Re}(Z_{f_1})}\, sin(2\pi f_1 t). \tag{10}$$

When two incident signals with different frequencies and different input powers are received by the tag, the total voltage is the superposition of two individual signal contributions using the same input impedance used in (10) as follows:

$$\begin{aligned} V_{in}(t) = &\sqrt{P_{\text{in},1} \cdot \text{Re}(Z_{f_1})}\, sin(2\pi f_1 t) \\ &+ \sqrt{P_{\text{in},2} \cdot \text{Re}(Z_{f_1})}\, sin(2\pi f_2 t). \end{aligned} \tag{11}$$

Multiple incident signals at the same frequency received by the tag are summated in a specific way that will be discussed later. The GUI makes use of a model to calculate the harmonic response of the tag using a two-region model for a harmonic radar transponder [8]. This models the output current of the transponder, through the Lambert function. The Lambert function is complex and multivalued. It calculates the complex solution to the equation:

$$f(z) = z\exp(z) = \text{W}(z\exp(z)), \tag{12}$$

where W denotes the use of the Lambert function. The model assumes that the transponder is ideally matched and rewrites the diode current $i_D(t)$ in terms of the dominant real equivalent impedance at the fundamental frequency Z_{f_1} using a modelled voltage source $v_{in}(t)$. The current flowing through the antenna and the load $i_T(t)$ can be said to be $i_T \approx i_D$, thus:

$$\begin{aligned} i_D(t) &= I_s\left(\exp\left(\frac{v_T(t)}{n_i V_T}\right) - 1\right) \\ &\approx i_T(t) = \frac{v_{in}(t) - v_T(t)}{\text{Re}(Z_{f_1})}, \end{aligned} \tag{13}$$

where I_s is the saturation current, $v_T(t)$ is the voltage across the diode, n_i is the diode ideality factor and V_T is the thermal voltage. By introducing $\rho = I_s Z_{f_1}/n_i V_T$ and $\text{w}(t) = \rho((i_T(t)/I_S) + 1)$, (13) can be rewritten to be solved using (12):

$$\text{w}\exp(\text{w}) = \rho\exp\left(\rho + \frac{V_{in}(t)}{n_i V_T}\right). \tag{14}$$

Using (14) and (13), the resulting diode current can ultimately be written as:

$$I_D(t) = I_s\, \frac{W\left(\rho\exp(\rho + \frac{V_{in}(t)}{n_i V_T})\right)}{\rho - 1}. \tag{15}$$

Calculating the voltage at the diode junction $V_j(t)$ follows as:

$$V_j(t) = n_i V_T\, ln\left(\frac{I_D(t)}{I_s + 1}\right). \tag{16}$$

The junction capacitance is dependent on (16) and is calculated using a separate time dependent function. The GUI adds the junction current, obtained by multiplying the junction capacitance C_j with the gradient of $V_j(t)$, to (15), for the total current:

$$I(t) = I_D(t) + C_j \nabla V_j(t). \tag{17}$$

The full current output in (17) includes all signal harmonics produced by the diode for $n \in [0, \infty)$. To compute the current at the frequencies of interest, an FFT is used to calculate the power spectrum in frequency domain $\iota(f_n)$, using bin size L.

$$\iota(f_n) = \frac{2|\text{FFT}(I(t))|}{L}, \tag{18}$$

where f_n is the output frequency. The code generalises that, for the harmonics, 20 times the frequency of f_1 can be used to represent all sinusoids accurately. This results in a resolution of 20480 for L and a sampling frequency of $f_s = 186.8\,\text{GHz}$. This results in a time length of roughly 0.11μs. Using (18), the spectral densities of the output current at the relevant output frequencies $I_{out}(f_n)$ is obtained as:

$$I_{out}(f_n) = \iota\left(\frac{f_n}{f_s/L} + 1\right)\beta_n, \tag{19}$$

where β_n is the corresponding current division coefficient, dependent on f_n. Of note is that β_n is calculated using the conjugated input impedance of the tag under the assumption that the antenna is fully matched to the diode. Calculating the output impedance of the tag Z_{f_n} at some frequency f_n yields the respective radiated power out of the tag:

$$P_{\text{rad}}(f_n) = \frac{1}{2}|I^2_{out}(f_n)|\,\text{Re}(Z_{f_n}). \tag{20}$$

Converting allows the reflected wave power from the tag to the radar to be expressed as:

$$P_{\text{rx}}(f_n) = P_{\text{rad}}(f_n) + G_{\text{out,D}} - \text{FSPL}(d, f_n) + G_{\text{rx}}, \tag{21}$$

where $G_{\text{out,D}}$ is the tag output antenna gain and G_{rx} is the receive antenna gain of the main radar. An example of a resulting heat map plotting the reflected power in dBm can be seen in Figure 2.

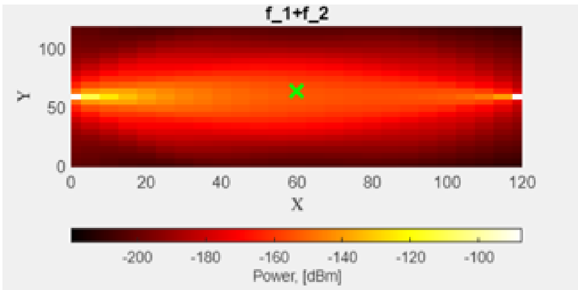

Fig. 2: Example heat map from GUI showing received power of the intermodulation signal at frequency f1+f2 depending on tag position in relation to main radar and helper node placement and orientation using [$X_{main} = 0$,$Y_{main} = 60$, $\theta = 0$] and [$X_h = 120$, $Y_h = 60$, $\theta_h = 180$] respectively

III-B Multiple helper set-up

The summation of multiple incident signals, at the same frequency received by the tag, needs to be calculated as a combination of signals coming from several sources. This is done under the assumption that the helpers are frequency synchronous, don't have different initial phases and have different accumulated phase offsets due to different propagation distances. This is achieved in the set-up by using GPS disciplined oscillators (GPSDOs), as the frequency lock is within 40 kHz at a 9.5 GHz carrier frequency [6]. Then (10) is recalculated as [9]:

$$V_a\, sin(x + \theta_a) + V_b\, sin(x + \theta_b) = V_c\, sin(x + \phi), \tag{22}$$

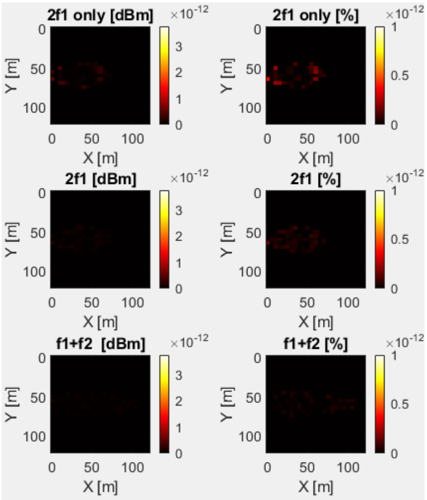

Fig. 3: Left, from top to bottom: dBm difference of improved code compared to GUI result for main radar only at $2f_1$, using one helper node at $2f_1$ and using one helper node at f_1+f_2. Right, from top to bottom: Percentage error of improved code compared to GUI result for main radar only at $2f_1$, using one helper node at $2f_1$ and using one helper node at f_1+f_2. Maximum error in region of interest approximately 6.3 e-14 dBm and 9 e-14%, due to numerical rounding errors.

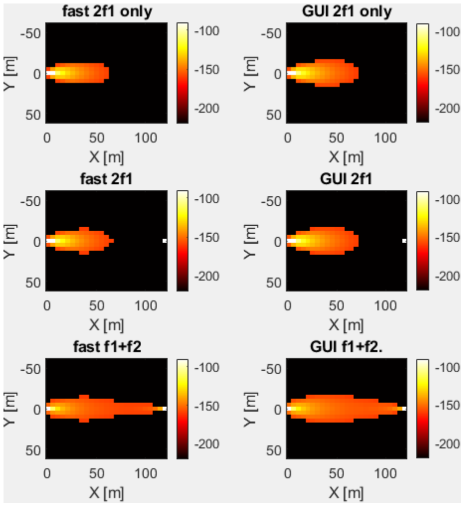

Fig. 4: Left, from top to bottom: Return power coverage area of faster approximation results for main radar only at $2f_1$, using one helper node at $2f_1$ and using one helper node at f_1+f_2. Right, from top to bottom: Return power coverage area results of original application for main radar only at $2f_1$, using one helper node at $2f_1$ and using one helper node at f_1+f_2.

where the relationships between the parameters are:

$$V_c^2 = V_a^2 + V_b^2 + 2\,V_a V_b\,cos(\theta_a - \theta_b); \tag{23}$$

$$\phi = arctan\left(\frac{V_a\,sin(\theta_a) + V_b\,sin(\theta_b)}{V_a\,cos(\theta_a) + V_b\,cos(\theta_b)}\right). \tag{24}$$

IV Improvements Initial Simulation Model

IV-A Single helper set-up

The speed of the GUI in calculating the power heat map for a fixed setup using one helper at the placement recorded in Table I was timed multiple times and averaged to be 92 seconds, not counting the start-up time. The number of possible combinations to be checked is expressed as the multiplication of the size of each parameter space:

$$S = |\overline{x}|\,|\overline{y}|\,|\overline{\theta}|, \tag{25}$$

where $|\overline{x}|$ is the parameter space of x, $|\overline{y}|$ is the parameter space of y and $|\overline{\theta}|$ is the parameter space of θ. The time required by the GUI to make S calculations using the settings as seen in Table I takes $1589760[s]$, which roughly equates to 609 days. This will be used as a base metric when talking about speed improvements onwards. Due to the expected calculation time, speed improvements were deemed priority number one to make optimisation through numerical calculation feasible.

Initially all iterative loops are changed to matrix manipulation. An adjustment was made to the size and index of the grid. When using a horn antenna oriented along the x-axis, the radiation pattern perpendicular to the x direction is significantly lower. The GUI imposes x onto the size of y, making the grid square, but also unnecessarily large in the y direction. Thus the size of x is decoupled from y to allow a smaller grid in calculations. Next, the main radar placement is fixed at ($x = 0$, $y = 0$, $\theta = 0$) instead of the placement used by the GUI ($x = 0$, $y = 60$, $\theta = 0$). This is so only the helper parameters are considered for optimisation and to simplify calculations for the distance between the main radar and other points in space.

After these optimisations, the output is compared against the GUI results to ensure that the calculations are still correct.

After the aforementioned steps to optimise the code, the same calculation for the fixed set-up using one helper is done, as with the GUI prior. The calculation speed improves to 14.4 seconds, which is roughly 6.4 times faster. The introduced error in dBm and in % due to the changed code, as can be seen in Figure 3, both do not exceed values of magnitude 10^{-13}. These errors are thought to exist due to numerical rounding differences.

The code optimisation yields a new calculation time of 248832 [s], or 2.88 days, which can be improved further. MATLAB's profile tool is used to determine which other parts of the code can be optimised, and returns that the Lambert function takes up roughly half of the computation time. Through the open source database of "Free Open Source Software mainly for Internet, Engineering and Science" [10], a faster Lambert function approximation was found written in C++. This was rewritten for use in MATLAB, together with other approximations it uses (i.e. $f = e^x$, $f = 2^x$ and $f = ln(x)$). The faster functions approximate the original functions by using smaller bit-lengths and using piecewise functions instead of the full Lambert function. Other approximations mainly use clever bit manipulation to approximate the result faster.

Deriving a relevant minimal power threshold level $P_{\mathrm{Rx,min}}$ using [6], the difference in results for the GUI and the speed improved calculations are seen in Figure 4. All grid points with return powers lower than $P_{\mathrm{Rx,min}}$ are set to black.

The results of using the approximation functions are seen in Figure 5. The calculation error when using the approximation has increased, staying within a maximum of 3.43 [dBm] or 2.58% error inside of the coverage calculation. However, the speed improvement is significant, as using this function drops the time to roughly 6 seconds. The calculation time using this approximation decreases with factors 15.3 and 2.4 that of the GUI and the code optimisation calculation times, respectively. Recalculating the optimisation time brings it down to 103680 seconds, (which is 1 day and 5 hours). Seeing as the resulting field holds within a 5% error rate, the speed improvement was chosen over the added error for use in further optimisation calculations. It also has to be mentioned that, in the coverage area, the error seems to be relatively homogeneous (roughly -3.1 [dBm], aside from the field fringes).

IV-B Multiple helper set-up

For optimisation purposes, three distinct cases for wave summation can be considered. One for average power, a worst case and a best case summation. These calculations use a predefined

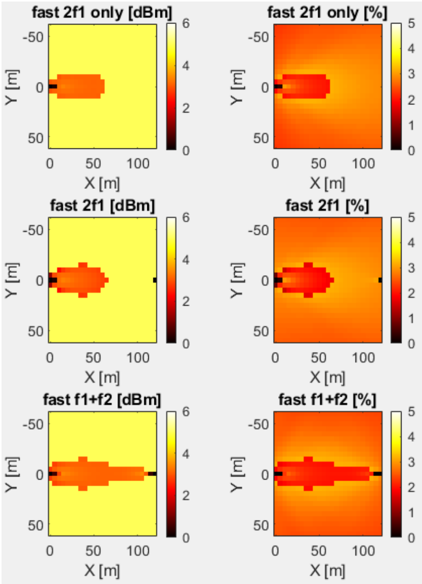

Fig. 5: Left, from top to bottom: dBm difference using approximation functions compared to original functions for main radar only at $2f_1$, using one helper node at $2f_1$ and using one helper node at $f_1 + f_2$. Right, from top to bottom: Percentage error using approximation functions compared to original functions for main radar only at $2f_1$, using one helper node at $2f_1$ and using one helper node at $f_1 + f_2$. Maximum error found in region of interest approximately 3.43 dBm and 2.58%, due to approximations.

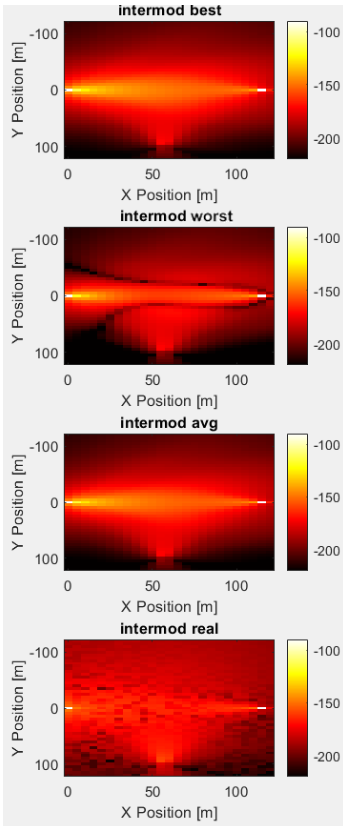

Fig. 6: Return power calculations for all cases given in (22) and (23); (Top to bottom:) best-case, worst-case, average-case and real-phase wave summation; Used in consideration of coverage area optimisation of the intermodulating signal at $f_1 + f_2$.

accumulated phase offset to give a simplified representation of these return signal scenarios. Each case is individually considered later for use in optimisation. These are calculated as:

$$\begin{aligned} V_{\text{c,avg}} &= V_a^2 + V_b^2, && \text{for } \phi = \pi/2; \\ V_{\text{c,worst}} &= V_a^2 + V_b^2 - 2\,V_a V_b, && \text{for } \phi = \pi; \\ V_{\text{c,best}} &= V_a^2 + V_b^2 + 2\,V_a V_b, && \text{for } \phi = 0. \end{aligned} \tag{26}$$

In Figure 6 the results specific to the cases discussed in (26) and for the real-phase signal are shown. The real-phase signal is calculated using (23) and (24) under the assumption of the signals being frequency synchronous, having no different initial phases, but having accumulated phase offsets.

The top three outputs show similar results, with the worst-case result showing a clear interference pattern. The real-phase case, there seems to be a vague indication of the interference seen in the second from the top result, the worst case calculation. As the wavelength is roughly of magnitude 1000 smaller than the resolution used in the calculation, the real phase does not seem to be reliable, as it depends on distance. Further considering robustness and coverage area representation for use in optimisation, the top result, (the best case), and real-phase case summations are disregarded. The worst case and third from the top, (the average case), summation results are therefore chosen for use in optimisation.

The error between the Lambert (left) and approximation function (right) for multiple helpers is shown in Figure 7. In comparison to the error when using one helper node, it is noticeable that the error seems to have gone down (now 1 dBm or 0.6% within the area of interest) and that the error seems equally homogeneous within the boundaries of the field fringes. This might indicate that some improvements in approximation could be made by comparison to the slower function for a specific number of helpers and power distribution over said helpers, but the need to fully research this is outside the scope of the current work.

V Helper Placement Optimisation

V-A *Problem Statement*

To be able to determine optimal placement for helper nodes, an objective function has to be created where the minimum or maximum is the ideal outcome for the problem presented. The coverage area of the intermodulation signal is expressed as:

$$J = -\frac{\Sigma[A_{\text{IM}}]}{N}, \tag{27}$$

where A_{IM} are points at which the power of the IR signal exceeds $\text{P}_{\text{Rx,min}}$ and N is the number of points evaluated in the calculation. This way, minimising (27) leads to the global optimum value. The viability of this depends on finishing within a feasible time-frame and the accuracy of the optimisation with respect to the global optimum.

The possibility of the first guess being correct P_{first} is written using (25) for the total field as used in the quantised model as:

$$P_{\text{first}} = \frac{1}{S} = \frac{1}{24 \cdot 24 \cdot 72} = \frac{1}{41472}. \tag{28}$$

This is restricted to some lower and upper bounds to disregard ranges outside of possible solution ranges. For instance, the range of $\overline{x}$ is bounded to be $[50, 120]$. The lower bound is where the harmonic return ends, therefore we aim further than this position. The upper bound is due to the fact that, for the radar transmission power used, the total possible distance is 120 meter in the first place. The bounds for the other parameters can similarly be reduced to $\overline{y} \in [-40, 40]$ and $\overline{\theta} \in [-150, 210]$. These restrictions are derived as an estimate due to the result of Figure 4 and the fact that, as previously mentioned, the main gain of the horn antenna is restricted mainly to $[-20, 20]$ degrees. These new bounds make the possibility of the first guess being correct:

$$P_{\text{first}} = \frac{1}{S} = \frac{1}{12 \cdot 20 \cdot 12} = \frac{1}{2880} \tag{29}$$

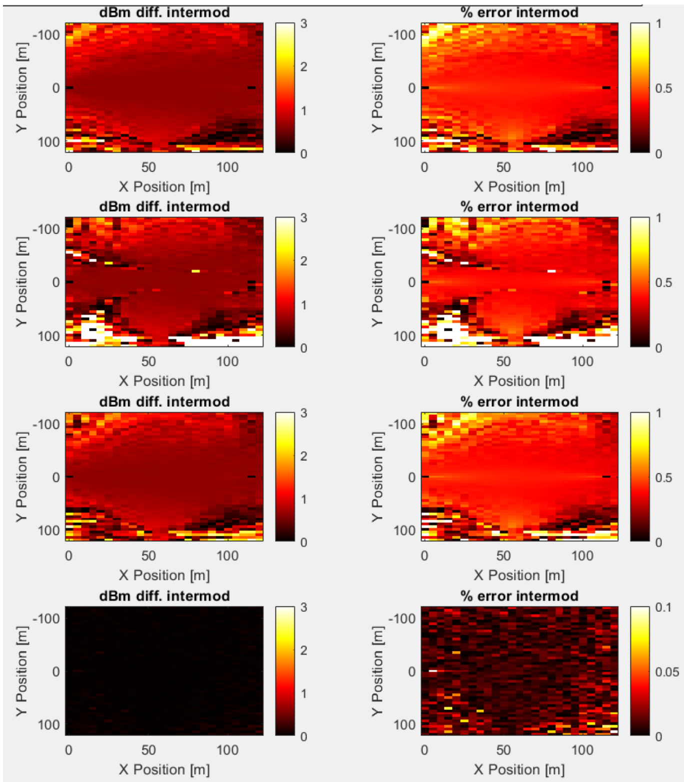

Fig. 7: Error of intermodulation signal at $f_1 + f_2$ between faster approximations and normal calculation; (Top to bottom:) best-case, worst-case, average-case and real-phase wave summation. Left: Error in [dBm]; Right: Error in [%]

Making use of the characteristic that SA mostly approximates the global optimum instead of always finding a singular global optimum, using the returned placement results as the new initial results can be utilised. For more helper nodes, the number of iterations and restarts using better initial guesses have to be adjusted to compensate an increase in combinations to speed up the optimisation.

As the search space S increases linearly with the number of helpers, two functions adjusting the upper and lower bounds are implemented. The first one activates when 85% of the maximum cost is reached and the second when 90% is reached. This function takes the best cost's parameters obtained from an optimisation run, if the cost exceeds a percentile threshold, and establishes new upper and lower bounds around that point:

$$\begin{aligned} \text{new bounds}_{85\%} &= [x_n \pm 5\,\mathrm{dX}, y_n \pm 5\,\mathrm{dY}, \theta_n \pm 5\,\mathrm{d}\theta]; \\ \text{new bounds}_{90\%} &= [x_n \pm 3\,\mathrm{dX}, y_n \pm 3\,\mathrm{dY}, \theta_n \pm 3\,\mathrm{d}\theta], \end{aligned} \tag{30}$$

where dX, dY and $\mathrm{d}\theta$ is the resolution used by the code to which the respective parameters are constrained. This should allow the chance of estimating global optima more accurately to increase following (25). The dynamic bounds function is the result after logging the average error away from the global optimum. In these tests the maximum average parameter error was found to be 5 for the 85% case and 3 for the 90% case. The resulting function is seen in Appendix C, under C.2.

Depending on the number of helpers, local optima will be able to form where linear algorithms can get stuck. Increasing helpers also multiplies the number of possible combinations, resulting in a large combinatorial problem. Thus, the main criteria for the optimiser are that it:

- is able to handle large combinatorial problems due to the large number of parameters;
- is able to escape local minima.

V-B *Simulated Annealing Optimisation*

Simulated Annealing (SA) is chosen as it can function for large combinatorial problems, such as the travelling salesman problem [11]. SA uses an algorithm to iteratively evaluate neighbouring solutions to some initial solution based on an objective function, usually called the cost function. This function is subject to some boundaries or constraints which are modelled as penalties or hard parameter bounds. New parameter combinations become a candidate for evaluation through an acceptance probability function [12]:

$$P_{\text{accept}}(\Delta J, \mathrm{T}) = \left(1 + \exp\left(\frac{\Delta J}{\mathrm{T}}\right)\right)^{-1} \tag{31}$$

where $\Delta J = J_{\text{best}} - J_{\text{new}}$ and T is the temperature that decreases over the number of iterations M, the initial temperature T_0 and the rate at which the temperature decreases, called the cooling schedule ϑ:

$$\mathrm{T} = \mathrm{T}_0 \vartheta^M \tag{32}$$

As the acceptance probability changes over the number of iterations, it plays a central role in the generation of new possible parameters. If the value for ϑ is too big or too small, it can cause the process to become stuck in local minima or to skip possibilities completely. Getting stuck in local minima can be prevented either by restarting the optimisation multiple times using the previous best guess as the initial guess, or by picking a more appropriate value for the cooling schedule. More helpers might also mean needing a larger value for the cooling schedule.

T_0 is estimated by picking a range for cost function J. This means that, the range of J needs to be re-scaled when the number of helpers changes. This is under the assumption that the coverage area will increase with an increase in helpers. This scaling is done manually for one, two and three helper nodes, where numbers beyond that are estimated based on the data available. Considering the starting situation, an initially high acceptance possibility P_0 is desired. Setting the highest possible cost $J_{max} = 250$ allows the calculation of the starting temperature, using a fractional value of J_{max}.

$$\mathrm{T}_0 = \frac{J_{max} \cdot 0.01}{\ln(P_0)} \approx \frac{2.5}{\ln(0.9)} \approx 25 \tag{33}$$

Again, by setting a final temperature value to be used $\mathrm{T}_{\text{Final}}$ and M, an indication for a value for ϑ is determined:

$$\vartheta = \left(\frac{\mathrm{T}_{\text{Final}}}{\mathrm{T}_0}\right)^{M^{-1}} = \frac{25}{2}^{50^{-1}} = 0.9595 \tag{34}$$

Values used for J_{max}, M, T_0 and $\mathrm{T}_{\text{Final}}$ are all subsequently changed iteratively, based on previous optimisation results for more than one helper, to allow a better indication of the global optimum. A simple verification of the optimisation where only the x coordinate is used as an optimisation parameter yields coordinates [115,0] with orientation 180 degrees (towards the main radar). This result is then verified by calculating and comparing for every x coordinate result.

When using multiple helpers, the optimiser gets stuck in local optima. Most notably, due to these local optima, the optimiser returns placements where the IR field exceeding $\mathrm{P}_{\mathrm{Rx,min}}$ is discontinuous between the main transmitter and some helper nodes. A penalty using the average case calculation is implemented to ensure that the intermodulating result is continuous between the radar and each helper node using a flood fill algorithm. This code is based on a well known algorithm, called flood-fill algorithm. Multiple restrictions are applied to the resulting coverage area in the form of penalties Q that add to the cost function:

$$J = -\frac{\Sigma[A_{\text{IM}}]}{N} + Q, \qquad (35)$$

where Q is scaled such that the maximum penalty it can add will at maximum be equal to the maximum obtainable cost, (so 250), to prevent forming of local minima. Adding this penalty leads to a realisation of calculation errors possibly propagating to the optimiser results. The code can be seen in Appendix C, under C.1. After implementation, the number of times the optimiser got stuck in local optima reduced significantly, as all results after had no discontinuity for the intermodulating field.

The resolution of the grid is found to interfere with optimiser results. This is because, despite the grid being bound to the resolution, the optimiser and its parameters were not. An example situation: using a resolution of 5 meters, the optimiser calculates the power into the tag at $[x_{tag} = 100, y_{tag} = 0]$ for some helper node at $[x_h = 105, y_h = 0, \theta_h = 180]$. However, due to the optimiser not being constrained to the grid, it chooses some point closer to the global optimum: $[x_{h,new} = 102.5, y_{h,new} = 2.5, \theta_{h,new} = 180]$. Furthermore, the horn antenna transmits a narrow beam, with a maximum gain of 15 dB, focused between [−20,20] degrees of its centre axis. The power resulting from the second iteration is thus attenuated due to this narrow beam.

This results in the optimiser adding more local minima, as now every point not on the grid likely yields worse results. In a conservative worst case scenario, the resulting guess has a potential 37 dB attenuation adding both potential FSPL and antenna gains. (This conservative guess is made by taking the worst possible result due to the horn antenna gain pattern and adding it to the average difference for FSPL for 5 and 2.5 meters). Additionally, the code in C.1 is not usable, as the helper node might not connect to the return field. A quantised version for SA was found on the MathWorks file exchange [13]. The code works by bounding new suggested candidates by the SA algorithm to the resolution. Some functions were changed to suit the cost function used.

VI Results

In the simulated scenarios using 1 to 4 helper nodes, the results from the optimiser were used to find the global optima. This was done under the assumption that the optimiser parameters are close to the global optimal parameter values; this will be tested using the first result for optimisation using 5 auxiliary helper nodes. All results use the same resolution (5[m]) and all transmission antennas use the same horn antenna gain of 15 dBi. All results also use a random initial parameter guess generated by MATLAB's rand function. Figure 8 is the harmonic return coverage using both the auxiliary power budget on top of the main radar power budget (200 Watt), which yields a coverage area of 2025 m^2. This will be used as a comparison metric for IR coverage area.

The results for Figures 10, 11, and 12 were found through the returned optimiser positions and orientations or by inspection around these optimiser return values. From Figures 9, 10, 11, and 12, the IR signal coverage areas are shown, with 2750 m^2, 2800 m^2, 2925 m^2, and 3125 m^2, respectively. These optimal results are used to fit a curve plotting the coverage area over the number of helpers used.

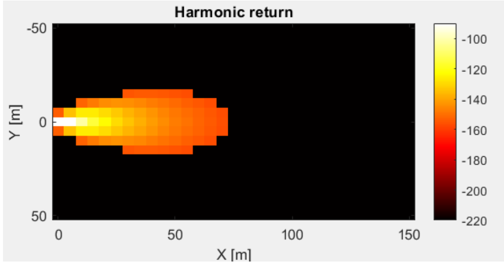

Fig. 8: Coverage area of HR return signal transmitting 53 dBm using no auxiliary helper nodes.

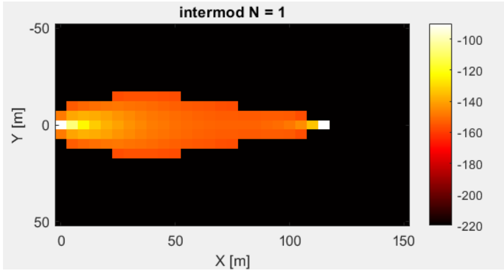

Fig. 9: Coverage area of IR return signal using one auxiliary helper node, position and orientation of helper node found by optimiser. Error from inspected global optimum is 0.0%.

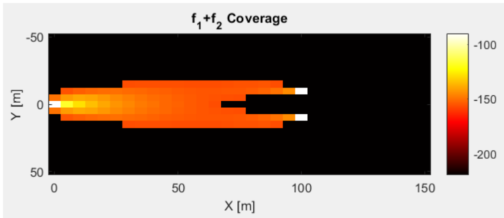

Fig. 10: Coverage area of IR return signal using two auxiliary helper nodes, position and orientation of helper nodes found by optimiser. Error from inspected global optimum is 0.9%.

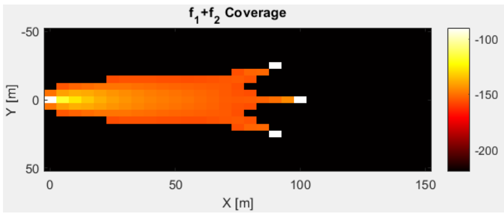

Fig. 11: Coverage area of IR return signal using three auxiliary helper nodes, position and orientation of helper nodes found by optimiser. Error from inspected global optimum is 0.0%.

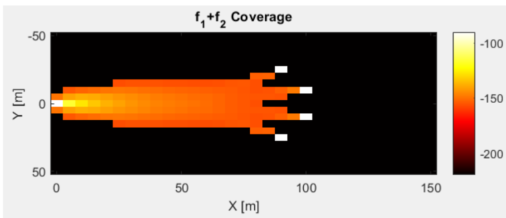

Fig. 12: Coverage area of IR return signal using four auxiliary helper nodes, position and orientation of helper nodes found by optimiser. Error from inspected global optimum is 3.2%.

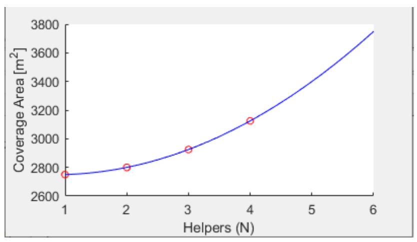

Fig. 13: Estimated coverage area over optimally placed and orientated number of helpers, using fitted curve $f(N) = 37.5N^2 - 62.5N + 2775$; N = number of helpers.

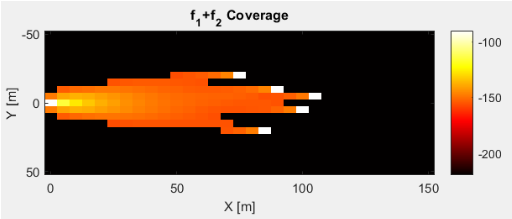

Fig. 14: Coverage area of IR return signal using five auxiliary helper nodes; position and orientation of helper nodes found by optimiser. Error from estimated global optimum returned by optimiser after single run is 12.4%.

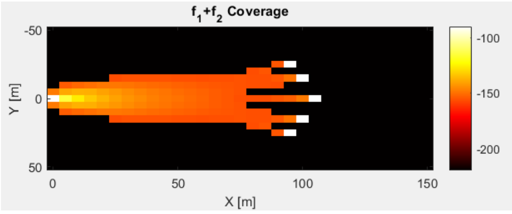

Fig. 15: Coverage area of IR return signal using five auxiliary helper nodes; new global optimum found using positions and orientations returned by optimiser. Error from estimated global optimum is 5.4%.

These points yield an approximation for the coverage area using $f(N) = 37.5N^2 - 62.5N + 2775$, as is shown in Figure 13.

To test the efficacy of the optimiser, it is chosen to compare the result the optimiser gives for 5 helper nodes to the theoretical area increase, which should result in a coverage area of 3400 m^2. Figure 14 shows the optimiser's single run result, returning the optimal IR signal coverage area found using five auxiliary helper nodes. The coverage area found by the optimiser is 3025 m^2.

Using the resulting positions and orientations to inspect symmetrical nodes, reflected through $y = 0$, allowed to find a coverage area of 3225 m^2. Figure 15 shows this new global optimum for the coverage area of the IR signal return using 5 helper nodes, forcing two symmetrical helper pairs from the previously obtained optimiser results. All optimiser and inspected results are compiled in Tables II and III. One can see the number of helper nodes used, the coverage area results for the IR signal using the optimiser, the (estimated) optimal IR area coverage, the error between the aforementioned two areas, and the time taken for the optimiser to run a single time. The HR coverage area from Figure 8 at equal power using 0 helper nodes is recorded for comparison. In Table II, the error of the optimiser increases as the number of helpers goes beyond 3. Using an equal power budget of 100 Watt for the main radar signal and 100 Watt distributed equally over all helper nodes, the IR area coverage increases by 0.91%, 6.36%, 13.64%, and an estimated 23.64% using two, three, four and five helper nodes respectively compared to the single helper case.

Using 100 Watt for the main radar signal and 100 Watt distributed equally over all helper nodes, the IR in comparison to the HR area coverage increases with 35.8%, 37.0%, 44.4%, 54.3%, by 59.3% using the positions and orientations found using one, two, three, four and five helper nodes, respectively, in comparison. In comparison to just the HR signal coverage area, as seen in Figure 8, using an equal power budget (200 Watt) and no helpers, the IR signal coverage area increase is more significant. This is due to the fact that using multiple low-power transmitters is cheaper than using a single high-power transmitter, as this requires significantly more direct current (dc) and much bigger antennas.

TABLE II: Comparison table between harmonic return signal coverage area using no helper nodes and optimal coverage areas found for intermodulating return signal using different number of helper nodes.

Number of helpers	0	1	2	3	4
Coverage area, [m^2]	2025	2750	2775	2925	3125
Optimal coverage, [m^2]	-	2750	2800	2925	3225
Error, [%]	-	0.0	0.9	0.0	3.2
Time optimisation [s]	-	186	658	1388	1612

TABLE III: Intermodulating return signal results using 5 helper nodes. On the left the results from a single optimisation run. On the right the optimal positions and orientations found through utilisation of single run optimisation by inspection using helper node pairs symmetrical through $y = 0$. Optimal coverage estimation from Figure 13

Optimal parameters through	Optimiser	Inspection
Number of helpers	5	5
Coverage area, [m^2]	3025[2]	3225[3]
Optimal coverage estimation, [m^2]	3400[1]	3400[1]
Error, [%]	12.4[1]	5.4 [3]
Time optimisation [s]	1836	-

VII Discussion

The overall optimisation up to four helper nodes is deemed a success. Beyond four helper nodes, the accuracy of the optimiser gives a clear indication of high coverage regions in parameter space after a single run. Utilising a second run, using the obtained best guess from the first run, will prove to be effective in obtaining more chances to bypass local minima, which lead to better guesses. The initial run accuracy could be further improved by multiple things, such as tuning the number of iterations, the cooling rate or starting temperature. Due to the relatively large resolution of the calculations, the error of the coverage area calculations is 6.25 m^2. Better performing hardware could use a smaller resolution, to increase guess accuracy, and use more iterations and a higher starting temperature, which will yield better results.

As is seen in Figure 13, the coverage area increases per added helper. However, as is seen from Figures 14 and 15, the coverage area seems to not increase as much by adding helpers as the initial data fitted curve suggests. Due to this, the question arises if the coverage area will keep increasing beyond 5 helpers, or if the fitted function needs to be adjusted.

Another question arises on the possibility of combining horn and other antenna gain patterns or using other gain patterns completely. Through inspection it is found that global optima seemingly yield position and orientation results for helper nodes that are symmetrical about the centre of the main radar orientation θ. A penalty implementation is able to make use of this through the optimiser and decrease the parameter search space at the same time, but was not made due to time constraints. Another question arises if there exists an optimum in a desired coverage area versus the power budget that is available to the system. An optimal power distribution over an arbitrary number of helpers can also be found using this optimiser, but was not implemented and tested due to time constraints.

VIII Conclusion

The optimal placement of auxiliary transmitters used in dual-mode X-band FMCW HR was done successfully for one to four auxiliary helper nodes. An optimiser was developed to determine optimal placement using simulated annealing. For five helper nodes, a single optimisation result is used to verify the viability of the optimiser. The area coverage of the HR signal using 53 dBm is used to compare IR coverage area increases at equal total power.

Implemented code improvements yield a speed increase of factor 6.4 to the initial GUI, with the calculation error introduced not exceeding 10^{-13}. The use of approximative function to calculate the return signal yields another factor 2.4 speed increase, relative to the previous speed increase. The calculation error increases when using various approximation functions, but stays within a maximum 2.58% inside the coverage area and seems to go down when the number of helper nodes are increased. In total, a speed increase of factor 15.3 over the initial model is obtained using approximated Lambert function.

With respect to the HR signal which uses equal power budget and no helpers, IR coverage area increases to 35.8%, 37.0%, 44.4%, 54.3% and by 59.3% by utilisation of one, two, three, four and five helper nodes, respectively.

Optimal estimated positions and orientations for up to five helper nodes have been found using the optimiser, with an error of 12.4% and 5.4%, utilising a single run optimisation result, and by inspection, from the projected global optimum in resulting coverage area, respectively.

The error of the optimiser increases with an increase in parameter search space. This might be due to the increase in combinations, which in turn forms more local optima. This suggests that further optimisation can be done to the optimiser parameters and process, which could improve the chance of escaping these local optima. Multiple improvements are discussed that could improve estimation accuracy and expand optimisation beyond its current scope.

Acknowledgements

This endeavour would not have been possible without Anastasia Lavrenko and Andrei Mogilnikov, who provided me both their expertise and time. I am especially grateful for the support my family offered during my studies and my friends and colleagues for their extensive help, moral support and overall existence.

References

[1] M. I. Skolnik. *Radar Handbook, Third Edition*. McGraw-Hill, 2008. ISBN: 978-0-07-148547-0.

[2] C. Wolff - radartutorial.eu. *The basic types of clutter*. 1998. URL: https://www.radartutorial.eu/11.coherent/co04.en.html.

[3] A. Mishra and C. Li. *A Review: Recent Progress in the Design and Development of Nonlinear Radars*. Ed. by dept. of Electrical and Texas Tech University Computer Engineering. 2021. URL: https://www.mdpi.com/2072-4292/13/24/4982.

[4] G. Storz, A. Lavrenko, J. Cavers, and G. Woodward. “Dual-Mode FMCW Harmonic Radar Supporting Auxiliary Transmitter Operation”. In: *IEEE International Radar Conference* (2021). DOI: 10.1109/RADAR54928.2023.10371040.

[5] everything RF. *What is the X-Band?* URL: https://www.everythingrf.com/community/x-band.

[6] R. Afroz, A. Lavrenko, G. Woodward, G. Storz, and S. Pawson. “Experimental Verification of Dual-Mode X-band FMCW Harmonic Radar”. In: *IEEE International Radar Conference* (2024). URL: https://www.researchgate.net/publication/384606140_Experimental_Verification_of_Dual-Mode_X-band_FMCW_Harmonic_Radar.

[7] A. Mishra and C. Li. *A Review: Recent Progress in the Design and Development of Nonlinear Radars*. 2021. URL: https://www.mdpi.com/2072-4292/13/24/4982.

[8] A. Lavrenko and J. Cavers. “Two-region model for harmonic radar transponders”. In: *Electronics Letters: Volume 56, Issue 16* (2020). DOI: 10.1049/el.2020.0779. URL: https://ietresearch.onlinelibrary.wiley.com/doi/10.1049/el.2020.0779.

[9] Wikipedia. *List of trigonometric identities*. 2025. URL: https://en.wikipedia.org/wiki/List_of_trigonometric_identities#Arbitrary_phase_shift.

[10] P. Mineiro. *The Free Open Source Software mainly for Internet, Engineering and Science Archive*. 2012. URL: https://fossies.org/.

[11] CMU School of Computer Science. *Simulated Annealing - Auton Technologies Glossary Index*. 2025. URL: https://www.cs.cmu.edu/afs/cs.cmu.edu/project/learn-43/lib/photoz/.g/web/glossary/anneal.html.

[12] Inc. The MathWorks. *How Simulated Annealing Works*. 2025. URL: https://nl.mathworks.com/help/gads/how-simulated-annealing-works.html.

[13] S. Hosseinzadeh. *Integer/Discrete Optimization with Simulated Annealing*. 2019. URL: https://nl.mathworks.com/matlabcentral/fileexchange/72539-integer-discrete-optimization-with-simulated-annealing?s_tid=prof_contriblnk.

APPENDIX A GLOSSARY: ABBREVIATIONS, TERMS AND SYMBOLS

- (radar) - Radio Detection and Ranging
- (EM) - Electromagnetic
- (Incident wave) - Wave direction from radar to load/target
- (Reflected wave) - Wave direction from load/target to radar
- (Dual-mode) - Radar system capable of operating using two return frequencies
- (FMCW) - Frequency modulated continuous wave
- (X-band) - RF operation range from 8 to 12 GHz.
- (HR) - Harmonic Radar
- (IR) - Intermodulating Radar
- (Chirp) - Compressed High-Intensity Radiated Pulse
- ($E(t)$) - Time dependent electric field [V]
- (Tag) - Harmonic radar transponder consisting of a half-wavelength planar dipole antenna, low barrier Schottky diode and a small inductive loop
- (k_n) - nth power coefficient term []
- ($s(t)$) - Arbitrary complex baseband waveform
- ($\mathrm{Re}\{x\}$) - Denotes real part of x
- (RF) - Radio Frequency
- (f_1) - Operating frequency main radar incident wave [Hz]
- (f_2) - Operating frequency auxiliary node incident wave [Hz]
- (Δf) - Frequency overlapping prevention term (=3B/2) [Hz]
- $(2f_1), (2f_2), (f_1 + f_2), (f_2 - f_1)$) - All relevant second order mixing product frequencies of reflected waves [Hz]
- (GUI) - Graphical user interface; name used to refer to initial simulation model
- (P_{tx}) - Transmit power of radar transmitter [dBm]
- (G_{tx}) - Transmit gain of radar transmitter [dBi]
- (FSPL(d, f) - Free space path loss [dB]
- ($G_{\mathrm{in,D}}$) - tag input antenna gain [dBi]
- (d) - Distance [m]
- (c) - Speed of light (2.99792e8) [$\frac{\mathrm{m}}{\mathrm{s}}$]
- (λ_n) - Wavelength of some frequency (c/f_n) [m]
- (P_{in}) - Signal power going into the tag [dBm or dBW]
- ($Z_{\mathrm{f_n}}$) - Impedance calculated at frequency f_n
- ($V_{\mathrm{in}}(t)$) - Electric field input amplitude into the tag [V]
- (W) - Denotes use of Lambert function
- ($i_D(t)$) - Diode current [A]
- ($v_{in}(t)$) - Modelled voltage source [V]
- ($i_T(t)$) - Current flowing through the antenna and the load [A]
- (I_s) - Saturation current [A]
- ($v_T(t)$) - Voltage across the diode [V]
- (V_T) - Thermal Voltage [V]
- (n_i) - Ideality factor of tag (I_D) - Resulting diode current using Lambert function [A]
- ($V_j(t)$) - Voltage at tag junction [V]
- (C_j) - Junction capacitance at tag junction [F]
- (∇) - Nabla operator []
- ($I(t)$) - Total current tag [A]
- (FFT) - Fast Fourier transform from time to frequency domain
- ($\iota(f_n)$) - Fast Fourier transform of current in tag [A]
- (L) - Bin size
- (f_s) - Sampling frequency [Hz]
- ($I_{out}(f_n)$) - Output current in tag at frequency f_n [A]
- (β_n) - Current division coefficient for frequency f_n []
- (Z_{f_n}) - Output impedance at some frequency f_n
- ($P_{\mathrm{rx}}(f_n)$) - Reflected signal power from tag to main radar [dBm]
- ($P_{\mathrm{rad}}(f_n)$) - Radiated power out of tag at frequency f_n [dBW]
- ($G_{\mathrm{out,D}}$) - Tag output antenna gain [dBi]
- (G_{rx}) - Receive antenna gain [dBi]
- (GPSDOs) - GPS disciplined oscillators
- (ϕ) - Accumulated phase offset due to different propagation distances of multiple waves
- (S) - All parameter combinations []
- ($|\overline{x}|$) - Denotes parameter space of optimisation parameter (x) []
- ($P_{\mathrm{Rx,min}}$) - minimal power threshold level [dBm]
- (J) - Resulting cost value from cost function []
- (A_{IM}) - Sum coverage area of intermodulating return signal [m^2]
- (N) - Total number of points considered in calculation
- (P_{first}) - Chance for first guess being global optimum over total parameter spaces. []
- (dX), (dY), (dθ) - Parameter resolutions used by the code for x, y and θ respectively [m], [m], [°]
- (SA) - Simulated Annealing
- ($P_{\mathrm{accept}}(J, \mathrm{T})$ - Acceptance probability function []
- (ΔJ) - Difference between best found cost result minus new result of cost function []
- (T) - Temperature (in SA) []
- (M) - Number of iterations []
- (T_0) - Initial temperature parameter []
- (ϑ) - Cooling schedule; Temperature cooling rate over iterations []
- (P_0) - High initial acceptance probability, chosen to allow parameter calculations []
- (J_{max}) - Maximum cost, chosen to allow parameter calculations []
- ($\mathrm{T}_{\mathrm{Final}}$) - Final temperature parameter []
- (Q) - Penalty used in cost function []
- ($f(N)$) - data fitted curve plotting coverage area estimation, where ($f(N) = 37.5N^2 - 62.5N + 2775$) [m^2]
- (dc) - Direct current []

APPENDIX B: GUI WITH SETTINGS RECORDED USED IN VERIFICATION

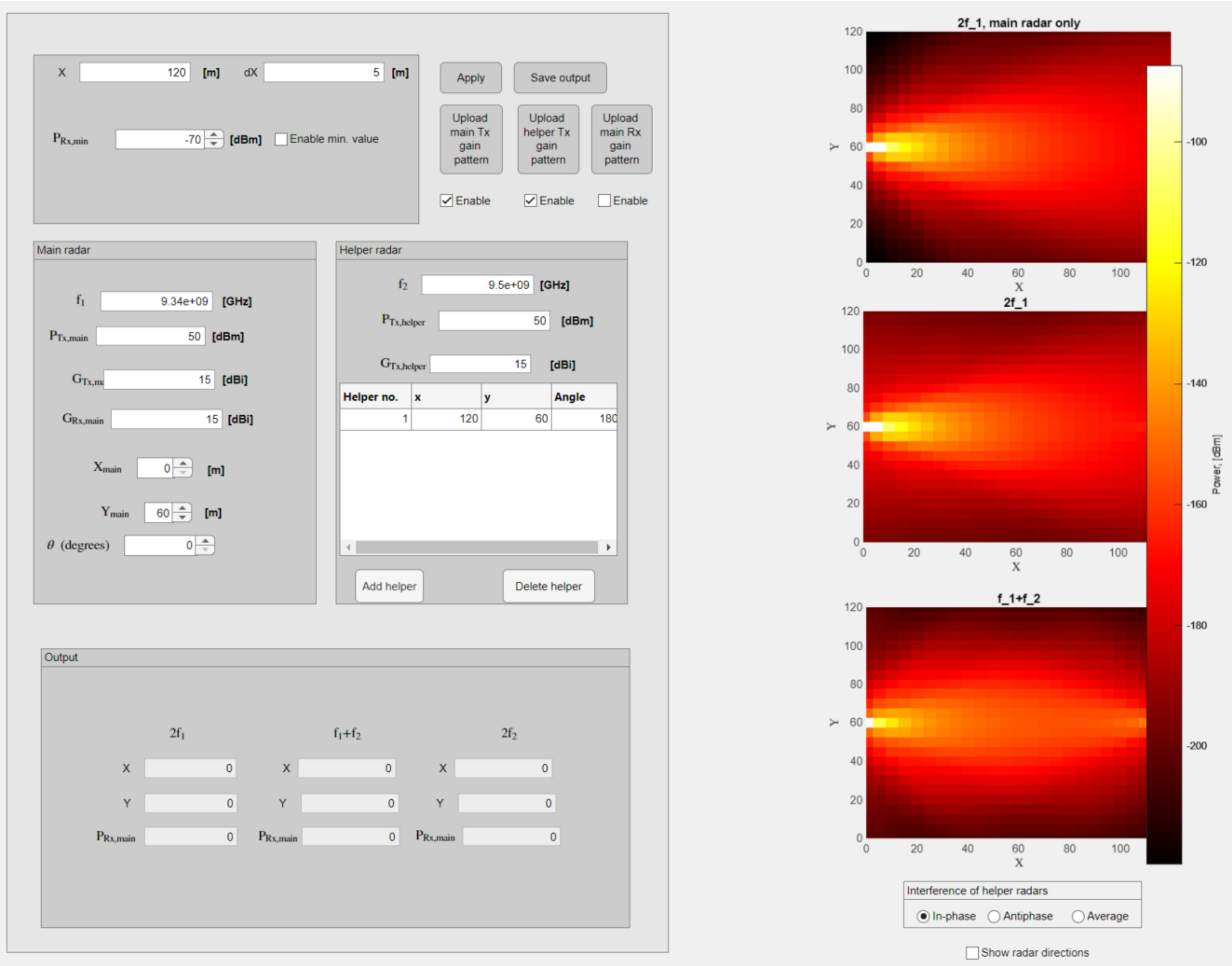

Fig. B.1: Example of GUI: (on the left) Parameter settings, (on the right) resulting heat maps for in-phase case (top to bottom) for main radar only, harmonic return intermodulating return signals

All parameters shown in Section III. Initial simulation model, Table I.

Appendix C: Functions written for optimiser

C.1 Continuity checking function using flood fill algorithm

```
function isConnected = findPath(Map, startcoord, endcoord)
    [rows, cols] = size(Map);
    visited = false(rows, cols);
    directions = [0, 1; 0, -1; 1, 0; -1, 0; 1, 1; 1, -1; -1, 1; -1, -1];

    function bigMemoryMoment(x, y)
        % Check if the current position is out of bounds or visited
        if x < 1 || x > rows || y < 1 || y > cols || visited(x, y) || Map(x, y) == 0
            return;
        end
        visited(x, y) = true;
        if x == endcoord(1) && y == endcoord(2)
            isConnected = true;
            return;
        end
        for i = 1:size(directions, 1)
            newX = x + directions(i, 1);
            newY = y + directions(i, 2);
            bigMemoryMoment(newX, newY);
            if isConnected
                return;
            end
        end
    end
    isConnected = false;
    bigMemoryMoment(startcoord(1), startcoord(2));
end
```

C.2 Boundary adjustment function

```
    function [lb_new, ub_new] = what_the_bounds_doin(x0_new, lb, ub)
    lb_new = [x0_new(:,1)-(25) ,x0_new(:,2)-(25) ,x0_new(:,3)-(25)];
    ub_new = [x0_new(:,1)+(25) ,x0_new(:,2)+(25) ,x0_new(:,3)+(25)];
    lbtruedoe = lb_new<=lb;      ubtruedoe = ub_new<=ub;
    lb_new = lb_new.*~lbtruedoe + lbtruedoe.*lb;
    ub_new = ub_new.*ubtruedoe + ~ubtruedoe.*ub;
end
```